Monthly Notices
of the
ROYAL ASTRONOMICAL SOCIETY

MNRAS **453,** 214–221 (2015) doi:10.1093/mnras/stv1623

Multiple AGN in the crowded field of the compact group SDSS J0959+1259

A. De Rosa,[1★] S. Bianchi,[2] T. Bogdanović,[3] R. Decarli,[4] R. Herrero-Illana,[5] B. Husemann,[6] S. Komossa,[7] E. Kun,[8,9] N. Loiseau,[10] Z. Paragi,[11] M. Perez-Torres,[5,12] E. Piconcelli,[13] K. Schawinski[14] and C. Vignali[15,16]

[1] *INAF/Istituto di Astrofisica e Planetologie Spaziali. Via Fosso del Cavaliere, I- 00133 Roma, Italy*
[2] *Dipartimento di Matematica e Fisica, Università degli Studi Roma Tre, via della Vasca Navale 84, I-00146 Roma, Italy*
[3] *Center for Relativistic Astrophysics, Georgia Institute of Technology, Atlanta, GA 30332, USA*
[4] *Max-Planck-Institut für Radioastronomie, Auf dem Hügel 69, D-53121 Bonn, Germany*
[5] *Instituto de Astrofísica de Andalucía (IAA-CSIC), E-18008 Granada, Spain*
[6] *European Southern Observatory Headquarters, Karl-Schwarzschild-St 2, D-85748 Garching, Germany*
[7] *Max-Planck-Institut für Radioastronomie, Auf dem Hügel 69, D-53121 Bonn, Germany*
[8] *Department of Experimental Physics, University of Szeged, Dóm tér 9, H-6720 Szeged, Hungary*
[9] *Department of Theoretical Physics, University of Szeged, Tisza Lajos krt 84–86, H-6720 Szeged, Hungary*
[10] *ESAC/XMM–Newton Science Operations Centre, Spain*
[11] *Joint Institute for VLBI ERIC, Postbus 2, NL-7900 AA Dwingeloo, The Netherlands*
[12] *Centro de Estudios de la Física del Cosmos de Aragón (CEFCA), E-44001 Teruel, Spain*
[13] *Osservatorio Astronomico di Roma (INAF), via Frascati 33, I-00040 Monte Porzio Catone(Roma), Italy*
[14] *Institute for Astronomy, Department of Physics, ETH Zurich, Wolfgang-Pauli-Strasse 27, CH-8093 Zurich, Switzerland*
[15] *Dipartimento di Fisica e Astronomia, Università degli studi di Bologna, Viale Berti Pichat 6/2, I-40127 Bologna, Italy*
[16] *INAF–Osservatorio Astronomico di Bologna, Via Ranzani 1, I-40127 Bologna, Italy*

Accepted 2015 July 15. Received 2015 July 8; in original form 2015 April 17

ABSTRACT

We present a multiwavelength study of a newly discovered compact group (CG), SDSS J0959+1259, based data from *XMM–Newton*, Sloan Digital Sky Survey (SDSS) and the Calar Alto optical imager BUSCA. With a maximum velocity offset of 500 km s^{-1}, a mean redshift of 0.035, and a mean spatial extension of 480 kpc, this CG is exceptional in having the highest concentration of nuclear activity in the local Universe, established with a sensitivity limit $L_X > 4 \times 10^{40}$ erg s^{-1} in 2–10 keV band and *R*-band magnitude $M_R < -19$. The group is composed of two type-2 Seyferts, one type-1 Seyfert, two LINERs and three star-forming galaxies. Given the high X-ray luminosity of LINERs which reaches $\sim 10^{41}$ erg s^{-1}, it is likely that they are also accretion driven, bringing the number of active nuclei in this group to five out of eight (AGN fraction of 60 per cent). The distorted shape of one member of the CG suggests that strong interactions are taking place among its galaxies through tidal forces. Therefore, this system represents a case study for physical mechanisms that trigger nuclear activity and star formation in CGs.

Key words: galaxies: active – galaxies: interactions – galaxies: Seyfert – X-rays: galaxies.

1 INTRODUCTION

Compact groups (CGs) are systems composed of a small number of galaxies (three or more) in a compact configuration with accordant redshifts, i.e. within 700 km s^{-1} from the group's mean velocity (Rose 1977; Hickson 1994, 1997). Some of the key open questions about CGs pertain to their relative importance in the universe and the relation between the global properties of these systems and the formation/evolution of their member galaxies (see the review by Hickson 1997). Because of their high galaxy densities, equivalent to those at the centres of rich clusters, and low velocity dispersions (about 200 km s^{-1}), CGs represent an environment where interactions, tidally triggered nuclear activity, and galaxy mergers are expected to be more prevalent than in other environments. This is found in the famous cases of CGs Hickson 16 (HCG 16; Ribeiro et al. 1996), Stephan's quintet (HCG 92; Stephan 1877), and Seyfert's sextet (HCG 79; Seyfert 1951). However, the level of nuclear activity in CGs has not been understood yet. In a systematic study of 280 galaxies in 64 HCG, Martínez et al. (2010)

★ E-mail: alessandra.derosa@iaps.inaf.it

Table 1. The sources of the CG in SDSS J0959+1259. (1) and (2) Right ascension and declination in degrees, position from SDSS. (3) Redshift derived from our analysis; the uncertainty is of the order of 300 km s^{-1}. (4) Offset line-of-sight velocity in km s^{-1} measured with respect to the mean velocity 10593 km s^{-1}. (5) Angular separation in arcsec with respect to the centre of the system (149.87°;13.03°). (6) Projected distance in kpc with respect to the centre assuming $H_0 = 70$ km s^{-1} Mpc^{-1}. (7) Unabsorbed 2–10 keV luminosity in 10^{42} erg s^{-1} derived from our analysis. (8) De-reddened (through Balmer decrement) [O III] luminosity in 10^{42} erg s^{-1} derived from our analysis. (9) Object type (see Section 3).

src	SDSS ID	RA (1)	DEC (2)	z (3)	δv (4)	Ang. sep (5)	Project dist. (6)	L_X (7)	L([O III]) (8)	Type (9)
1	J095906.68+130135.4	149.778	13.026	0.037	463	327	227	5	0.07	Sy2
2	J095903.28+130220.9	149.764	13.039	0.036	183	377	262	0.12	0.003	LINER
3	J095908.95+130352.4	149.787	13.064	0.0339	317	318	221	0.1	0.0008	LINER
4	J095912.19+130410.5	149.801	13.070	0.0337	395	280	195	<0.3	0.002	SFG
5	J095914.76+125916.3	149.812	12.988	0.034	208	259	180	2.8	0.4	Sy2
6	J095859.91+130308.4	149.749	13.052	0.035	227	430	299	<0.2	0.008	SFG
7	J095900.42+130241.6	149.752	13.045	0.035	20	418	290	<0.1	0.02	SFG
8	J095955.84+130237.7	149.983	13.043	0.035	30	389	270	15	0.03	Sy1

used optical emission-line ratios to classify the type of nuclear activity. They established that 28 per cent of sample galaxies are AGN (37 per cent being Seyfert-like and the remainder LINERs), 15 per cent are transition objects (TO), and 20 per cent are the star-forming galaxies (SFG).

Similarly, Silverman et al. (2014) used *Chandra* and *XMM–Newton* data to select 18 galaxy groups with mass $M_{\rm group} \sim 10^{13}$ M$_{\odot}$ and redshift $z \sim 0.05$. The groups account for 2–30 galaxies each and were observed down to a sensitivity limit of $L_X > 10^{40}$ erg s^{-1} and B band mag <18. They found 16 AGN/LINERs distributed in 18 groups, implying a mean number of AGN/LINERs per group less than 1 (more precisely, 0.89 ± 0.22).

The system discussed in this paper, associated with the SDSS J0959+1259 at redshift $z = 0.035$, has already been recognized as the only quintuplet detected in a sample of 1286 multiple AGN/LINER systems (Liu et al. 2011). The galaxies in this field that constitute our group have projected separations of $\lesssim$100 h^{-1} kpc and the line-of-sight velocity differences of $\lesssim$500 km s^{-1} (Hickson 1997). Within these criteria, we find seven spectroscopically identified sources which are listed in Table 1 (sources 1–7). We also find another source in this region (src8), which is close in redshift ($z = 0.035$) but at larger projected separation, and include it in this study.

The group in SDSS J0959+1259 satisfies the criteria used by Hickson (1997) to define a CG:

(i) population: it is composed by more than four galaxies with absolute magnitudes within 3 mag of the brightest (Table 3);

(ii) isolation: the radius of the smallest circle containing all the galaxies in the group (about 6.5 arcmin in our CG, see Table 1) is at least three times smaller than the distance from the group centre to the nearest unrelated galaxy with the absolute magnitude within 3 mag of the brightest member. Using NED data base[1] we find that the nearest such galaxy (with accordant redshift) is located at about 21 arcmin from the centre of the CG;

(iii) compactness: the mean brightness surface of the group in the R band, calculated by distributing the flux of the member galaxies over the smallest circular area containing their geometric centres, is ∼26 mag arcsec^{-2} (29 mag arcsec^{-2} including src8).

The mean redshift of the CG is $\langle z \rangle = 0.0353$ and the mean velocity is $\langle v \rangle = 10\,593$ km s^{-1}. The centre of this field has RA 09$^{\rm h}$59$^{\rm m}$28$^{\rm s}$.97 and Dec. 13°01′53″.0, and the average distance of sources from the geometric centre of the group is 240 kpc. The X-rays (left) and optical (right) images of the CG are shown in Fig. 1.

In this paper, we present a detailed optical and X-ray study of the CG in SDSS J0959+1259. The observations and data analysis are presented in Sections 2 and 3, respectively, and results are discussed in Section 4. Throughout this work, we assume $H_0 = 70$ km s^{-1} Mpc^{-1}, $\Omega_\Lambda = 0.7$, $\Omega_{\rm M} = 0.3$, and AB magnitudes. Errors and upper limits quoted in the paper correspond to the 90 per cent confidence level, unless noted otherwise.

2 OBSERVATIONS AND DATA REDUCTION

2.1 SDSS

All galaxies in our CG are targeted with SDSS under the legacy programme GALAXY (Strauss at al. 2002). We retrieved the SDSS-III DR12 spectra for all them (see Table 1) from the survey web page.[2] The SDSS spectra are shown in Fig. 2. The emission-line flux of all the primary diagnostic lines (H β, [O III] λ5007, [O I] λ6300, H α, [N II] λ6583, and [S II] $\lambda\lambda$6713, 6732) were measured on top of the stellar continuum using the package PYPARADISE (Husemann et al., in preparation) and listed in Table 2. PYPARADISE models the stellar continuum as a superposition of template stellar population spectra from the CB07 library (Bruzual & Charlot 2003) after normalizing both the SDSS and the template spectra with a running mean over 100 pix, interpolating regions with strong emission lines. A simple Gaussian kernel is used to match the template spectra to the line-of-sight velocity distribution. The line fluxes are then inferred by fitting the Gaussian line profiles coupled in redshift and intrinsic rest-frame velocity dispersion. Errors are obtained using a bootstrap approach where 100 realizations of the spectrum were generated based on the pixel errors with just 80 per cent of the template spectra and modelled again with the same approach (at fixed stellar kinematics).

2.2 BUSCA

We observed SDSS J0959+1259 using the multiband camera BUSCA on the 2.2 m telescope in Calar Alto observatory. These observations span the whole optical window from U to I over a 12 arcmin × 12 arcmin field of view. The throughput curves of the

[1] https://ned.ipac.caltech.edu/

[2] http://skyserver.sdss3.org/dr12

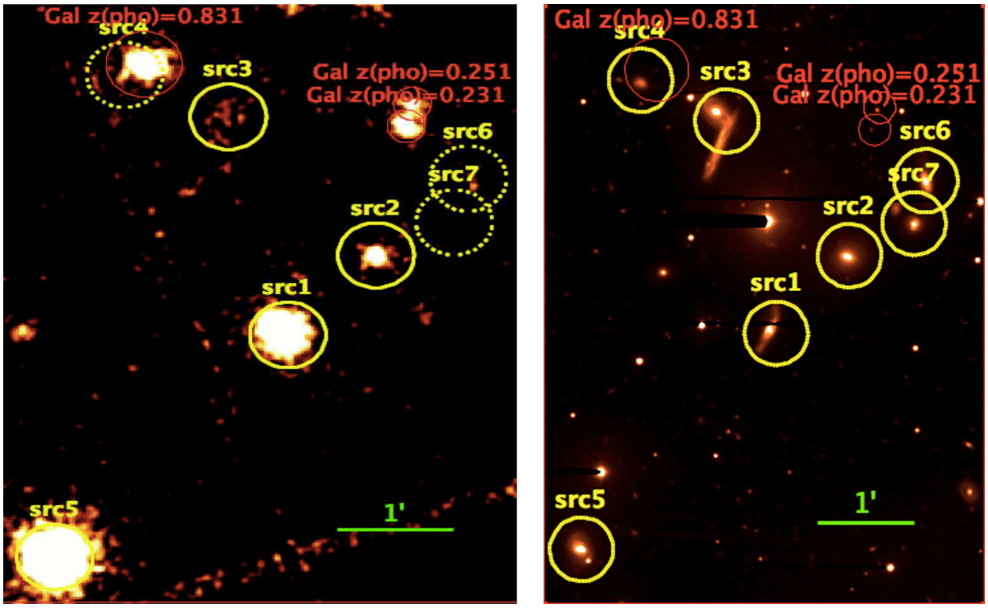

Figure 1. Left: *XMM*-EPIC smoothed mosaic image of the CG region (pn, MOS1 and MOS2 co-added). North is up and east is to the left. src8 (NGC 3080) is off the plot, 10 arcmin to the east from src1. Yellow thick circles show the group sources listed in Table 1. Undetected sources are shown with dashed line. Red thin circles are the sources in the field not included in our group, that lack a spectroscopic redshift in the SDSS (our estimated photometric redshifts based on BUSCA images suggest that they are background objects). Right: the BUSCA *R*-band colour image of the same region on the left. Labels are the same.

dichroic mirrors, convolved with the detector efficiency, roughly correspond to those of the SDSS u, r, $i + z$, and Johnson B filters. Five 12 min-long frames were collected in each band, dithered by a few arcsec in order to clean our final images from cosmic rays and bad pixels. Data were processed with our own IRAF-based pipeline `redbusca`. The astrometric solution was computed via ASTROMETRY.NET (Lang et al. 2010). The photometric calibration was obtained by comparing instrumental magnitudes of field stars with SDSS photometry, and assuming colour corrections to account for differences in the filter throughput curves, as described in Mazzucchelli et al. (in preparation). The 10σ detection limits for a point source are 25.76, 25.84, 25.56, 24.40 mag in U, B, R, and I, respectively. The seeing in R band was 1.0 arcsec. We created photometric catalogues using SEXTRACTOR (Bertin & Arnouts 1996). We base our source identifications on the R-band image, which is more sensitive, and measure forced photometry on the other images based on the R-band input apertures. We obtain the stellar mass $M_\star$ and star-forming rate (SFR) estimates, listed in Table 3, by fitting the available BUSCA+SDSS broad-band photometry using the SED fitting software MAGPHYS (da Cunha, Charlot & Elbaz 2008). BUSCA observations are about a factor of 9 deeper than SDSS, which has a limiting sensitivity of 22.0, 22.2, 22.2, 21.3, and 20.5 mag in u, g, r, i, and z, respectively (the SDSS average seeing is about 1.43 arcsec).

2.3 *XMM–Newton*

XMM–Newton observed the field around SDSS J0959+1259 on 2007 November 15 (ObsID: 0504100201) with a nominal exposure of 22 ks. Both EPIC cameras (MOS and pn) were observing in full-frame mode (thin filter). Data were reduced using SAS v13.5 with standard settings and the most updated calibration files available at the time of the data reduction.

The sources in the *XMM* field were detected using the EPIC source finding threads `edetect chain`, on five images in the 0.3–0.5, 0.5–1, 1–2, 2–4.5, and4.5–12 keV energy bands with a detection threshold of 3σ. Sources src1, src2, src3, src5, and src8 are clearly detected in all bands. src8 and src5 have already been identified in X-rays as Seyfert-like AGN earlier (LaMassa et al. 2009; Baumgartner et al. 2014). src6 and src7 are not detected (3σ confidence level), while the X-ray emission visible in the *XMM–Newton* composite image at a distance of ∼13 arcsec from src4 is likely due to a background quasar at $z = 0.831$. All spectra were extracted from circular regions with 30 arcsec radius which include more than 80 per cent of the source counts at 1.5 keV in the EPIC cameras. The background spectra were extracted in the same CCD chip from circular regions free from contaminating sources and of the same size as the regions containing a source.

After screening selection and filtering for the flaring events, the net exposure for the EPIC cameras is 17.5 ks. Each spectrum (and associated background) was rebinned in order to have at least 25 counts for each background-subtracted spectral channel and not to oversample the intrinsic energy resolution by a factor larger than 3. The X-ray spectra of the sources detected with *XMM–Newton* are shown in Fig. 4. Spectral fits for pn and (co-added) MOS cameras were performed in the 0.3–10 keV energy band.

3 THE CROWDED ENVIRONMENT IN THE FIELD OF SDSS J0959+1259

The CG SDSS J0959+1259 is shown in Fig. 1, where the composite EPIC-pn and MOS12 (left-hand panel) and the R-band BUSCA images (right-hand panel) are presented. src8 (NGC 3080), which is located 10 arcmin to the east from src1, is not shown. Yellow thick circles indicate CG sources, the dashed yellow circles mark the three objects not detected in X-rays, while the red thin circles show the background sources in the field not related to the group.

The fluxes of the optical emission lines of the sources in the CG are listed in Table 2 and the most common emission-line diagnostic diagrams are shown in Fig. 3. All three diagrams lead to a consistent

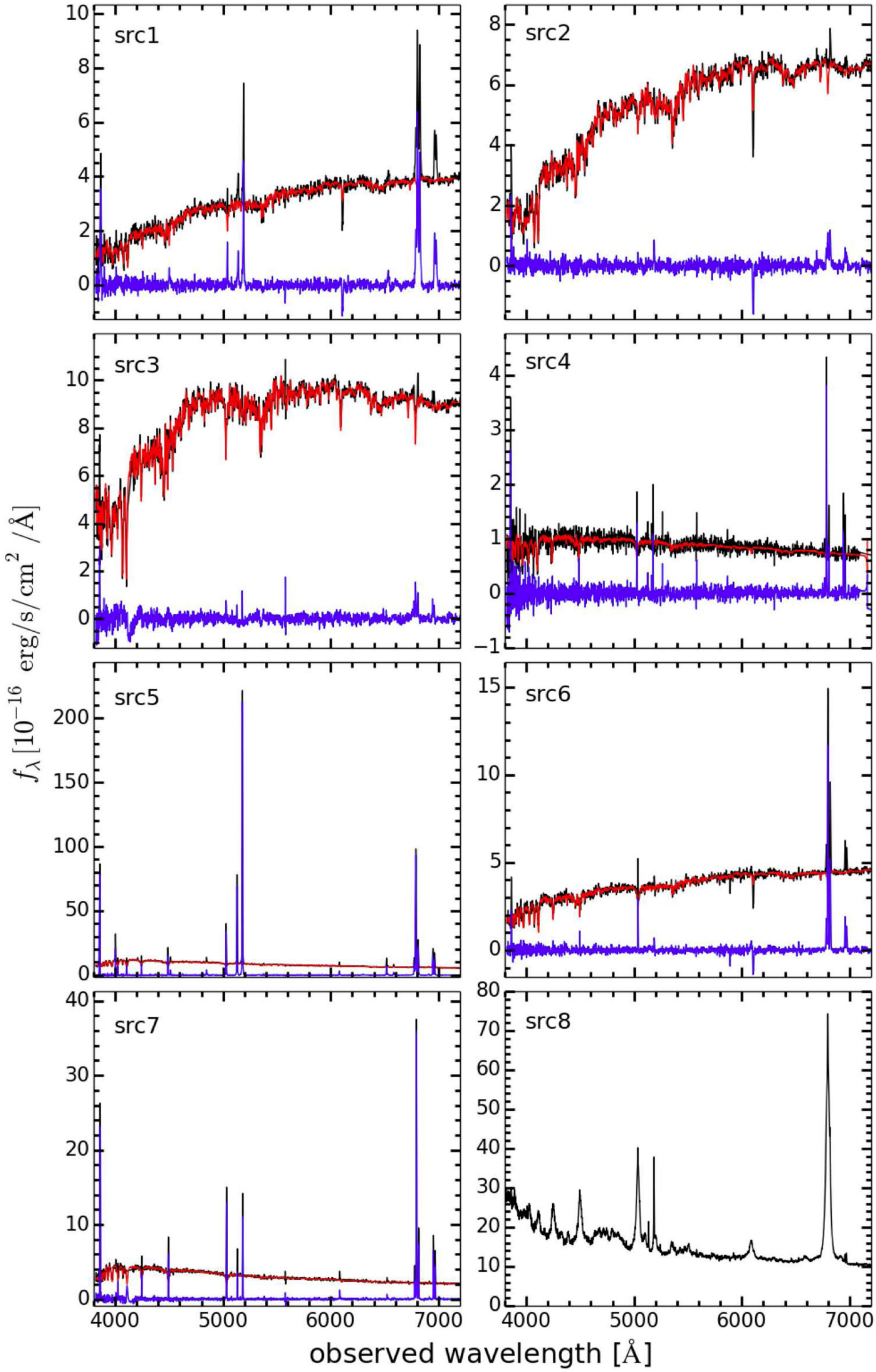

Figure 2. SDSS spectra of the sources in the field of SDSS J0959+1259. Composite spectrum (in black), model fit from the starlight subtraction (red), and starlight-subtracted spectrum (blue).

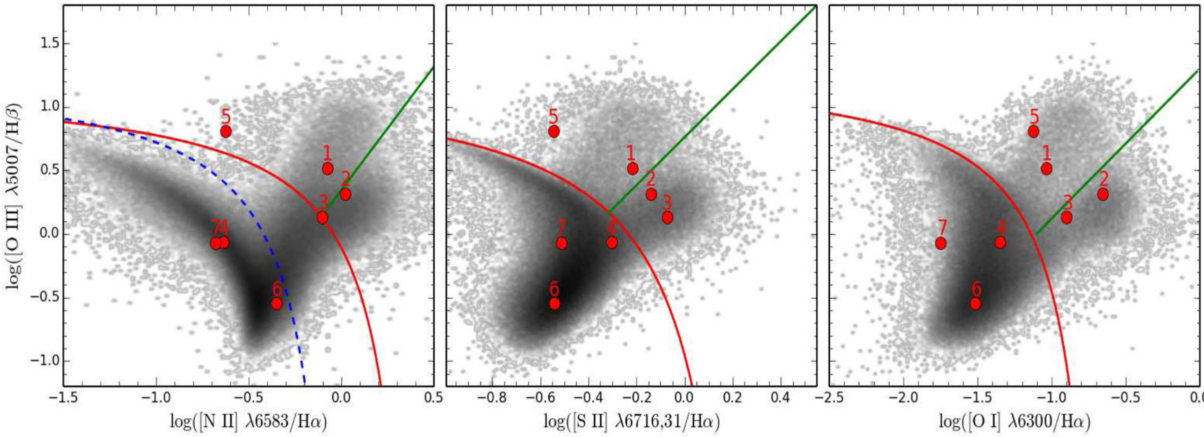

Figure 3. Position of src1 to scr7 in the most common emission-line ratio diagnostic diagrams. Errors bars for these high S/N spectra are smaller than the symbol size. SDSS galaxies are shown in grey. Red solid line marks the maximum line starburst as inferred by Kewley & Dopita (2002), the blue dashed line represents the empirical SFG boundary proposed by Kauffmann et al. (2003), and the green solid line is the empirically proposed division between AGN and LINERs.

Table 2. Optical emission lines. The fluxes are in 10^{-16} erg cm^{-2} s^{-1} at the rest wavelength of the lines. See details in Section 2.1.

src	H β 4861 Å	[O III] 4960 Å	[O III] 5007 Å	[O I] 6300 Å	[N II] 6548 Å	H α 6563 Å	[N II] 6583 Å	[S II] 6717 Å	[S II] 6730 Å	Type
1	10.7	11.6	35.2	5.8	17.5	63.2	53.1	20.7	17.6	Sy2
2	3.4	2.3	7.1	2.6	4.1	11.8	12.4	4.6	3.9	LINER
3	4.7	2.1	6.3	1.4	2.9	11.1	8.8	5.9	3.6	LINER
4	5.0	1.4	4.3	0.78	1.3	17.6	4.0	5.4	3.4	SFG
5	162.9	343.8	1041.8	41.7	43.5	555.5	131.8	87.8	70.8	Sy2
6	15.9	1.5	4.5	2.7	13.1	88.9	39.6	14.3	11.3	SFG
7	51.9	14.7	44.5	3.1	12.0	173.4	36.4	31.7	21.6	SFG

Table 3. BUSCA data analysis results. See details in Section 2.2. (1) Stellar mass in $M_\odot$. (2) Star-forming rate in $M_\odot$ yr^{-1}. (3) R-band absolute magnitude. (4) I-band absolute magnitude.

src	log $M_\star$ (1)	SFR (2)	M_R (3)	M_I (4)
1	9.36	20	−20.3	−21.0
2	10.85	<1	−21.1	−21.8
3	10.52	<1	−20.7	−21.3
4	9.30	<1	−18.7	−19.2
5	10.01	65	−20.7	−21.1
6	10.51	150	−20.4	−21.1
7	9.29	5	−19.6	−20.1

classification of objects into two Seyfert 2s, two LINERs, and three SFGs. The optical spectrum of src8 shows broad Balmer emission lines (FWHM ∼ 750 km s^{-1}) and thus, points to a type-1 Seyfert.

It is worth noting that our classification of src6 and src7 departs from that by Liu et al. (2011), who report them as broad-line AGN. In order to examine the spectra for presence of the broad lines we fit the spectra with the narrow-line components and inspect the residuals. These show no evidence for broad lines. Moreover, we find that the narrow lines ratios point to a classification of src6 and src7 as SFGs (Fig. 3). It is possible that the mismatch is a consequence of a standard automatic procedure used by Liu et al. (2011) to classify a large number of sources in their sample.

The results of the X-ray spectral analysis are presented in Table 4 and best-fit spectra are shown in Fig. 4. The 0.3–10 keV spectra of the two Seyfert 2s (src1 and src5) are modelled with an absorbed power law plus a thermal component with temperature of $kT \sim$ 0.1–0.6 keV (`mekal` in XSPEC) emerging below 2 keV. The cold absorption gas has column densities in the range $N_{\rm H} \approx 1$–20×10^{22} cm^{-2}. In the Seyfert 1 source (src8) the broad-band spectrum is well fitted with an absorption component with partial covering fraction $f_{\rm c} = 0.41 \pm 0.07$. The partial covering model is favoured with respect to a fully covering cold absorption with an F-test probability larger than 99.9 per cent.

A narrow Fe Kα emission line is also measured in the three Seyferts, with an equivalent width of ∼100–130 eV. These are the brightest objects of the system in both the X-ray and optical wavebands. The range of luminosity of the Seyferts is 10^{42}–10^{43} erg s^{-1}, that is in very good agreement with the values found in the studies of larger samples of local AGN (e.g. CAIXA; Bianchi et al. 2009).

The two LINERs (src2 and src3) are modelled with a power-law continuum in the X-ray band. Both LINERs are unabsorbed and show no detectable Fe line, although the S/N is poor above 5 keV due to their X-ray flux (less than 10 net counts in the pn). Their 2–10 keV luminosity is nevertheless high. At $\sim 10^{41}$ erg s^{-1}, it is above the mean value found in the systematic X-ray study of the largest sample of LINERs (González-Martínez et al. 2009). This study clearly shows that AGN sources have higher luminosities in 2–10 keV band ($\log L_X = 40.22 \pm 1.24$) than non AGN-like sources ($\log L_X = 39.33 \pm 1.16$). This is a strong indication that LINERs in this CG may be accretion driven.

Table 4. X-ray spectral analysis. Combined EPIC-pn and MOS12 data. See details in Section 2.3. (1) Total 0.3–10 keV pn counts in 10^{-2} s^{-1}. (2) Absorption column density in 10^{22} cm^{-2}. (3) Photon index. (4) Temperature of the thermal emitting plasma. (5) Equivalent width of the narrow Fe emission line in eV. (6) Unabsorbed 0.5–2 keV luminosity in 10^{42} erg s^{-1} (fraction due to the thermal component in parenthesis). (7) Unabsorbed 2–10 keV luminosity in 10^{42} erg s^{-1}. (8) 2–10 keV observed flux in 10^{-12} erg cm^{-2} s^{-1}.

src	Counts (1)	$N_{\rm H}$ (2)	Γ (3)	kT (4)	EW (Fe Kα) (5)	$L_{\rm soft}$ (6)	$L_{\rm hard}$ (7)	$F^{\rm obs}_{2-10\,{\rm keV}}$ (8)
1	5.8 ± 0.2	13^{+2}_{-2}	1.5 ± 0.3	$0.6^{+0.1}_{-0.2}$	100 ± 60	2.7 ± 0.1 (2 per cent)	5.3 ± 0.1	0.89 ± 0.01
2	0.9 ± 0.1	<0.2	$1.3^{+0.6}_{-0.4}$	–	–	0.04 ± 0.01	0.12 ± 0.05	0.04 ± 0.02
3	0.77 ± 0.09	$1.0^{+1.0}_{-0.6}$	1.7^{a}	$0.4^{+0.2}_{-0.1}$	–	0.08 ± 0.01 (25 per cent)	0.11 ± 0.02	0.04 ± 0.01
5	20.1 ± 0.4	$0.77^{+0.06}_{-0.06}$	1.91 ± 0.08	$0.11^{+0.07}_{-0.02}$	130 ± 80	2.2 ± 0.1 (1 per cent)	2.8 ± 0.1	0.94 ± 0.03
8	220 ± 1	$^{b}14^{+5}_{-4}$	2.41 ± 0.02	–	73 ± 40	22.6 ± 0.1	14.7 ± 0.2	3.7 ± 0.1

Notes. ^{a}Fixed value. This value has been fixed in the spectral fit. ^{b}The best-fit model requires a partially covering absorber, with coverage fraction $f_{\rm c} = 0.41 \pm 0.07$.

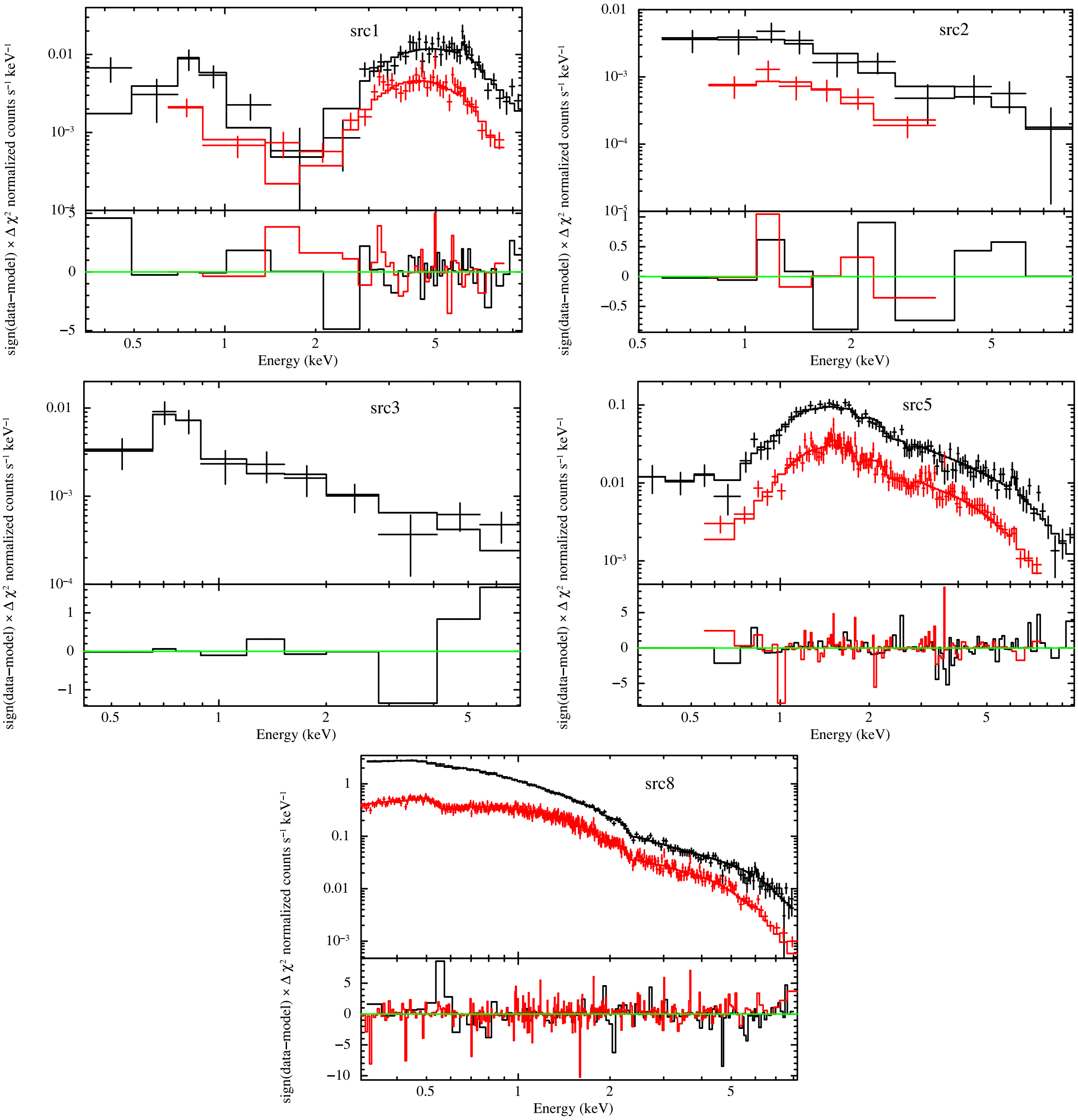

Figure 4. *XMM*-pn (black) and MOS12 (red) co-added data of the sources detected in the region of SDSS J0959+1259. From top left src1, src2, src3, src5 and src8 is shown in the last panel. Bottom panels show residuals of the best-fit models and our data set (see details in Section 3). No strong residuals are present across the whole energy band.

None of the SFGs (src4, src6, src7) are detected by *XMM–Newton*, placing a 3σ upper limit on flux in 2–10 keV of about 1.4$\times$ 10^{-14} erg cm^{-2}s^{-1}. This corresponds to a luminosity of $\sim$4 $\times$ 10^{40} erg s^{-1}, assuming a photon index 1.7, and absorbing column density of 10^{22} cm^{-2}.

4 DISCUSSION AND CONCLUSIONS

The CG in SDSS J0959+1259 represents one of the best examples of exceptionally strong nuclear activity in CGs in the nearby Universe. The combined optical and X-ray analysis clearly shows that this system is formed by two type-2 Compton-thin Seyferts, one type-1 Seyfert, two LINERs, and three SFGs.

In terms of spectral components and shape, the X-ray behaviour of LINERs (src2 and src3) is in very good agreement with the global properties of the sample of LINERs investigated in X-rays by González-Martínez et al. (2009). However, in terms of 2–10 keV luminosity, both src2 and src3 show high values ($\sim$$10^{41}$erg s^{-1}) that is within the average value found for the AGN candidates.

We conclude that our LINERs are likely accretion driven, which increase the fraction of AGN in this CG to from 40 to 60 per cent (from three to five out of eight). The only other example of an AGN-rich group like this is the well-known HCG 16 (Ribeiro et al. 1996; Turner, Reeves & Ponman 2001), with an AGN fraction of 75 per cent (three out of four galaxies).

Note that fibre collision bias in SDSS survey is an important effect (Li et al. 2006), in fact there is a limit of 55 arcsec to how close two fibres can be on the same tile. Consequently $\sim$10 per cent of targeted galaxies from a photometric catalogue cannot be assigned fibres and obtain measured spectroscopic redshifts. However, all brightest galaxies of the CG discussed here were spectroscopically observed by SDSS, implying that we cannot be missing AGN because of fibre collisions. On the other hand, other groups with similar AGN fraction may remain undetected due to this well-known effect. In this work, we are not aiming at a statistical study of the incidence of CG with high AGN fractions, but rather reporting the detection of such a unique group.

We compared our result with a systematic analysis of a sample of CGs with mass $M_{\rm group}$ $\sim$ 10^{13} M$_{\odot}$, investigated in X-rays with a limiting luminosity L_X > 10^{40} erg s^{-1} and *B* band mag <18 (Silverman et al. 2014). The number of AGN in our group is significantly higher than the mean number of 0.89 $\pm$ 0.22 AGN/LINERs per group found by Silverman et al. (2014), with a similar L_X and M_R selection. The AGN fraction found in their analysis was 36^{+14}_{-11} per cent and 13^{+9}_{-4} per cent for galaxies classified as central or satellite, respectively.

In order to find how common is the level of activity found in the GC analysed here, we also compare it to several other environments at low and high redshift. For example, rescaling our results for their adopted X-ray luminosity and *R*-band magnitude limits (L_X > 10^{42} erg s^{-1} and M_R < $-$20), we find that the our AGN fraction is 40 per cent, i.e. higher than the estimates of the AGN fraction of galaxies in the field (1.19 $\pm$ 0.11 per cent; Haggard et al. 2010). Our AGN fraction is also higher than that measured in isolated galaxies (7–20 per cent; Sabater et al. 2008). Using similar magnitude selection, and rescaling our results for their adopted X-ray luminosity limits, the AGN fraction in SDSS J0959+1259 is 60 per cent, i.e. higher than found in clusters (2–5 per cent, with M_R < $-$20 and L_X > 10^{41} erg s^{-1}; Martini et al. 2006). In high-z galaxies (0.25 < z < 1.05) with mass $M_\star$ >2.5 $\times$ 10^{10} M$_{\odot}$, the AGN fraction with an X-ray luminosity limit L_X > 10^{42} erg s^{-1} is of about 10 per cent (Silverman et al. 2011). These galaxies are commonly found in kinematic pairs characterized by physical separations less than 75 kpc and a line-of-sight velocity difference less than 500 km s^{-1}. In SDSS J0959+1259, the fraction of AGN with L_X above 10^{42} erg s^{-1} is 40 per cent, significantly higher with respect to the sample of high-z galaxies.

Using SFR versus stellar mass relation at z = 0, we find the values of SFR for src6 and src7 (see Table 3) higher than measured in the local Universe (Elbaz et al. 2007). This indicates an enhanced star formation, which is especially evident in src6. In addition, the fraction of the SFG galaxies in this CG is 38 per cent (three out of eight), while in HCGs the percentage is around 20 per cent (Martínez et al. 2010).

The values of the specific star formation rate (which is a measure of the relative growth rate of the galaxy) obtained with BUSCA data for the Seyfert 2s, is about 2.5 Gyr^{-1} (see Table 3), in good agreement with values measured in larger samples of AGN in the local Universe (Elbaz et al. 2007; Rovilos et al. 2012). The detection of a thermal component in the Seyfert 2s is highly significant, at >99.9 per cent confidence (see Table 4), and it contributes about 1–2 per cent to the total luminosity in 0.5–2 keV ($L_{\rm th}$ $\sim$2–5 $\times$ 10^{40} erg s^{-1}). This component is likely due to the emission from the narrow-line regions (Bianchi & Guainazzi 2007); however, we cannot exclude a possibility that it is due to a nuclear SF component. Using the relation from Ranalli, Comastri & Setti (2003), we obtain an upper limit for the nuclear SFR of about 20 and 10 M$_{\odot}$ yr^{-1} for src1 and src5, respectively.

The Arecibo HI survey ALFALFA (Giovanelli et al. 2005) shows a very large amount of H I gas in this group (2 $\times$ 10^{10} M$_{\odot}$). It is unclear whether its origin is intergalactic, as found in other CGs (Koribalski, Gordon & Jones 2003), or intragalactic, but it apparently could provide enough material to fuel the AGN and SFGs. In this scenario, the broad-line region detected in src8 can in principle be formed by gas enrichment. The ALFALFA survey has recently been used to show that H I has disturbed morphologies (tails and bridges) in post-merger galaxies while it exhibits an abundance similar to isolated galaxies (Ellison et al. 2015). The distorted shape of the edge-on disc galaxy (src1 in Fig. 1) already suggests that strong interactions are occurring among the galaxies in the CG mediated by the tidal forces or ram pressure of the intragroup medium. Furthermore, src5 exhibits an extraordinary low [N II]/H α ratio (the error on this ratio for type 2 AGN is much lower than the spectral offset found, see Fig. 3), but is clearly a Compton-thin AGN. This is very rare in the local Universe (Groves, Heckman & Kauffmann 2006), and it could be due to a recent galaxy interaction or due to accretion of low-metallicity gas from the intragroup environment.

The high incidence of AGN in this CG point to favourable conditions for inducing the black hole growth. However, the accretion rate in M$_{\odot}$ yr^{-1} estimated from accretion luminosity (L_X) is relatively low, so the activity cannot be simply explained by the presence of gas. The enhanced nuclear activity, the presence of SFGs and the proximity of the CG allow detailed, spatially resolved mapping of the distribution and kinematics of the stellar and gaseous components with the Multi Unit Spectroscopic Explorer (MUSE, with a proposal by our team already approved). This makes the system a good case study for physical mechanisms that trigger AGN and star formation in CGs.

ACKNOWLEDGEMENTS

We thank the anonymous referee for his/her helpful comments which improved the manuscript. All coauthors, members of the

MAGNA project (http://www.issibern.ch/teams/agnactivity/Home.html), gratefully acknowledge support of the International Space Science Institute (ISSI) in Bern, Switzerland. TB acknowledges the support from the Alfred P. Sloan Foundation under grant no. BR2013-016 and the National Science Foundation under grant no. NSF AST-1211677. Funding for SDSS-III has been provided by the Alfred P. Sloan Foundation, the Participating Institutions, the National Science Foundation, and the U.S. Department of Energy Office of Science. The SDSS-III web site is http://www.sdss3.org/. SDSS-III is managed by the Astrophysical Research Consortium for the Participating Institutions of the SDSS-III Collaboration including the University of Arizona, the Brazilian Participation Group, Brookhaven National Laboratory, Carnegie Mellon University, University of Florida, the French Participation Group, the German Participation Group, Harvard University, the Instituto de Astrofisica de Canarias, the Michigan State/Notre Dame/JINA Participation Group, Johns Hopkins University, Lawrence Berkeley National Laboratory, Max Planck Institute for Astrophysics, Max Planck Institute for Extraterrestrial Physics, New Mexico State University, New York University, Ohio State University, Pennsylvania State University, University of Portsmouth, Princeton University, the Spanish Participation Group, University of Tokyo, University of Utah, Vanderbilt University, University of Virginia, University of Washington, and Yale University.

This research has made use of the NASA/IPAC Extragalactic Database (NED) which is operated by the Jet Propulsion Laboratory, California Institute of Technology, under contract with the National Aeronautics and Space Administration.

REFERENCES

Baumgartner W. H., Tueller J., Markwardt C. B., Skinner G. K., Barthelmy S., Mushotzky R. F., Evans P. A., Gehrels N., 2014, ApJS, 207, 19
Bertin E., Arnouts S., 1996, A&A, 317, 393
Bianchi S., Guainazzi M., 2007, in Angelo Antonelli L., Luca Israel G., Piersanti L., Tornambe A., Burderi L., Di Salvo T., Fiore F., Matt G., Teresa Menna M., eds, AIP Conf. Proc. Vol. 924, The Multicolored Landscape of Compact Objects and their Explosive Origins. Am. Inst. Phys., New York, p. 822
Bianchi S., Guainazzi M., Matt G., Fonseca Bonilla N., Ponti G., 2009, A&A, 495, 421
Bruzual G., Charlot S., 2003, MNRAS, 344, 1000
da Cunha E., Charlot S., Elbaz D., 2008, MNRAS, 388, 1595
Elbaz D. et al., 2007, A&A, 468, 33
Ellison S. L., Fertig D., Rosenberg J. L., Nair P., Simard L., Torrey P., Patton D. R., 2015, MNRAS, 448, 221
Giovanelli R. et al., 2005, AJ, 130, 2598
González-Martín O., Masegosa J., Marquez I., Guainazzi M., Jimenez-Bailon E., 2009, A&A, 506, 1107
Groves B. A., Heckman T. M., Kauffmann G., 2006, MNRAS, 371, 1559
Haggard D., Green P. J., Anderson S. F., Constantin A., Aldcroft T. L., Kim D. -W., Barkhouse W. A., 2010, ApJ, 723, 1447
Hickson P., 1994, ApJ, 427, 684
Hickson P., 1997, ARA&A, 35, 357
Kauffmann G. et al., 2003, MNRAS, 346, 1055
Kewley L. J., Dopita M. A., 2002, ApJS, 142, 35
Koribalski B., Gordon S., Jones K., 2003, MNRAS, 339, 1203
LaMassa S. M., Heckman T. M., Ptak A., Hornschemeier A., Martins L., Sonnentrucker P., Tremonti C., 2009, ApJ, 705, 568
Lang D., Hogg D. W., Mierle K., Blanton M., Roweis S., 2010, AJ, 139, 1782
Li C., Kauffmann G., Jing Y. P., White S. D. M., Börner G., Cheng F. Z., 2006, MNRAS, 368, 21
Liu X., Shen Y., Strauss M. A., Hao L., 2011, ApJ, 737, 101
Martínez M. A., Del Olmo A., Coziol R., Perea J., 2010, AJ, 139, 1199
Martini P., Kelson D. D., Kim E., Mulchaey J. S., Athey A. A., 2006, ApJ, 644, 116
Ranalli P., Comastri A., Setti G., 2003, A&A, 399, 39
Ribeiro A. L. B., De Carvalho R. R., Coziol R., Capelato H. V., Zepf S. E., 1996, ApJ, 463, L5
Rose J., 1977, ApJ, 211, 311
Rovilos E. et al., 2012, A&A, 546, 58
Sabater J., Leon S., Verdes-Montenegro L., Lisenfeld U., Sulentic J., Verley S., 2008, A&A, 486, 73
Seyfert C. K., 1951, PASP, 63, 371
Silverman J. D. et al., 2011, ApJ, 743, 2
Silverman J. D., Miniati F., Finoguenov A., Carollo C. M., Cibinel A., Lilly S. J., Schawinski K., 2014, ApJ, 780, 67
Stephan M. E., 1877. MNRAS, 37, 334
Strauss M. A. et al., 2002, AJ, 124, 1810
Turner M. J. L., Reeves J. N., Ponman J. T., 2001, A&A, 365, L110

This paper has been typeset from a TEX/LATEX file prepared by the author.